

Shadowing Effects on the Nuclear Suppression Factor, $R_{d\text{Au}}$, in d+Au Interactions

R. Vogt

Nuclear Science Division, Lawrence Berkeley National Laboratory, Berkeley, CA 94720, USA

and

Physics Department, University of California, Davis, CA 95616, USA

Abstract

We explore how nuclear modifications to the nucleon parton distributions affect production of high transverse momentum hadrons in deuteron-nucleus collisions. We calculate the charged hadron spectra to leading order using standard fragmentation functions and shadowing parameterizations. We obtain the d+Au to pp ratio both in minimum bias collisions and as a function of centrality. The minimum bias results agree reasonably well with the BRAHMS data while the calculated centrality dependence is a stronger function of p_T than the data indicate.

One of the most intriguing results from the Relativistic Heavy Ion Collider (RHIC) at Brookhaven National Laboratory has been the suppression of hadrons with high transverse momentum, p_T , in central Au+Au collisions at center-of-mass energies, $\sqrt{S_{NN}}$, of 130 and 200 GeV. The AA suppression factor,

$$R_{AA}(p_T) = \frac{d\sigma_{AA}/dp_T}{\langle \sigma_{NN}^{\text{in}} T_{AA} \rangle d\sigma_{pp}/dp_T} , \quad (1)$$

compares the AA and pp hadron p_T distributions, normalized by the number of binary collisions, the product of the nucleon-nucleon inelastic cross section, σ_{NN} , and the nuclear overlap function T_{AA} . Saturation effects in the initial nuclear wavefunction and final-state parton energy loss were both proposed as explanations of the large suppression seen in Au+Au collisions by PHENIX [1,2], STAR [3,4] and BRAHMS [5]. To determine whether the suppression is an initial or final-state effect, d+Au collisions at $\sqrt{S_{NN}} = 200$ GeV were recently studied at RHIC. The data [6–8] show that, at midrapidity ($\eta \approx 0$), the d+Au suppression factor,

$$R_{\text{dAu}}(p_T) = \frac{d\sigma_{\text{dAu}}/dp_T}{\langle \sigma_{NN}^{\text{in}} T_{\text{dAu}} \rangle d\sigma_{pp}/dp_T} , \quad (2)$$

is much closer to unity. These results suggest that the strong suppression in Au+Au collisions is a final-state effect, implying that, at least at central rapidities, saturation effects are small. However, at higher rapidities where the nuclear parton momentum fraction, x_2 , is smaller, such effects might still be important. Since x is not very small at RHIC, it is necessary to check if other, more conventional, models of nuclear shadowing may also explain the data.

The BRAHMS collaboration has measured R_{dAu} at several values of pseudorapidity, η , and observed increasing suppression as η increases from $|\eta| \leq 0.2$ to $\eta = 3.2$ [8]. The BRAHMS measurements are in four η bins: $|\eta| \leq 0.2$; $0.8 \leq \eta \leq 1.2$ ($\eta = 1$); $1.9 \leq \eta \leq 2.35$ ($\eta = 2$) and $2.9 \leq \eta \leq 3.5$ ($\eta = 3.2$), corresponding to center-of-mass scattering angles, θ_{cm} , of $101.4^\circ \leq \theta_{\text{cm}} \leq 78.6^\circ$, $48.4^\circ \leq \theta_{\text{cm}} \leq 33.5^\circ$, $17.01^\circ \leq \theta_{\text{cm}} \leq 10.9^\circ$ and $6.3^\circ \leq \theta_{\text{cm}} \leq 3.5^\circ$ respectively. These data have also been divided into three centrality bins, (0 – 20)%, (30 – 50)% and (60 – 80)%, equivalent to $0 \leq b \leq 3$ fm, $4 \leq b \leq 5$ fm and $5.5 \leq b \leq 6.3$ fm.

fm respectively. The results in the two lowest η bins are reported for $(h^+ + h^-)/2$ while the $\eta = 2.2$ and 3.2 bins are reported for h^- only where h^+ and h^- stand for the positively and negatively charged hadron multiplicities respectively.

In this paper, we calculate $R_{\text{dAu}}(p_T)$ in the BRAHMS η bins using two parameterizations of nuclear shadowing. We also calculate the central-to-peripheral ratios, $R_{\text{CP}}(p_T)$, with two parameterizations of the spatial dependence of shadowing. The calculated ratios are compared to the BRAHMS data [8]. To better illustrate the effects of shadowing alone, we do not include the Cronin effect, p_T broadening [9,10], in our calculations.

We make a leading order (LO) calculation of minijet production to obtain the yield of high- p_T partons [11]. The p_T distribution of Ref. [12] is modified to include the nuclear parton distribution functions,

$$\frac{d\sigma_{\text{dAu} \rightarrow hX}}{d^2b dp_T} = 2p_T \sum_{i,j=q,\bar{q},g} \int_{\theta_{\min}}^{\theta_{\max}} \frac{d\theta_{\text{cm}}}{\sin \theta_{\text{cm}}} \int dx_1 \int dx_2 \int d^2s \int dz \int dz' \\ \times F_{i/\text{d}}(x_1, Q^2, \vec{s}, z) F_{j/\text{Au}}(x_2, Q^2, |\vec{b} - \vec{s}|, z') \frac{D_{h/k}(z_c, Q^2)}{z_c} \frac{d\hat{\sigma}_{ij \rightarrow k}}{d\hat{t}} \quad (3)$$

where x_1 and x_2 are the parton momentum fractions in the deuterium and gold nuclei respectively, Q is the momentum scale of the hard interaction and z_c is the fraction of the parton momentum transferred to the final-state hadron. The integrals over center-of-mass scattering angle, $\theta_{\min} \leq \theta_{\text{cm}} \leq \theta_{\max}$, correspond to the BRAHMS angular regions, given previously. The $2 \rightarrow 2$ minijet cross sections, $d\hat{\sigma}_{ij \rightarrow k}/d\hat{t}$, are given in Ref. [13]. Even though the next-to-leading order corrections may affect the shape of the p_T distributions, the higher-order corrections should largely cancel out in R_{dAu} , as is the case for J/ψ [14] and Drell-Yan [11] production.

The parton densities in the gold nucleus, $F_{j/\text{Au}}(x, Q^2, \vec{b}, z)$, can be factorized into x and Q^2 independent nuclear density distributions, position and nuclear-number independent nucleon parton densities, and a shadowing function, $S_{\text{P,S}}^i(A, x, Q^2, \vec{b}, z)$, that describes the modification of the nuclear parton distributions in position and momentum space. The first subscript on the shadowing function, P, refers to the shadowing parameterization while the second, S, to the spatial dependence. Most available shadowing parameterizations ignore

effects in deuterium so that $F_{i/d}$ depends only on the deuterium density distribution and the nucleon parton densities. We account for the proton and neutron numbers of both nuclei. Then [14]

$$F_{i/d}(x, Q^2, \vec{s}, z) = \rho_d(\vec{s}, z) f_{i/N}(x, Q^2) \quad (4)$$

$$F_{j/Au}(x, Q^2, |\vec{b} - \vec{s}|, z') = \rho_{Au}(|\vec{b} - \vec{s}|, z') S_{P,S}^j(Au, x, Q^2, |\vec{b} - \vec{s}|, z') f_{j/N}(x, Q^2) \quad (5)$$

where $f_{i/N}(x, Q^2)$ is the nucleon parton density. In the absence of nuclear modifications, $S_{P,S}^j \equiv 1$. The nucleon density distribution of the gold nucleus is assumed to be a Woods-Saxon with $R_{Au} = 6.38$ fm [15]. We use the Hulthén wavefunction [16] to calculate the deuteron density distribution. The densities are normalized so that $\int d^2s dz \rho_A(\vec{s}, z) = A$. We use the MRST LO parton distributions [17] for isolated nucleons and take $Q^2 = p_T^2$.

We have chosen two parameterizations of nuclear shadowing which cover extremes of gluon shadowing at low x . The Eskola *et al.* parameterization, EKS98, is based on the GRV LO [18] parton densities. At the minimum scale, Q_0^2 , valence quark shadowing is identical for u and d quarks. Likewise, \bar{u} and \bar{d} shadowing is identical at Q_0^2 . Even though the light quark shadowing ratios are not constrained to be equal at higher scales, the differences between them are small. Shadowing of the heavier flavor sea, \bar{s} and higher, is calculated separately at Q_0^2 . The shadowing ratios for each parton type are evolved to LO for $2.25 < Q^2 < 10^4$ GeV and are valid for $x \geq 10^{-6}$ [19,20]. Interpolation in nuclear mass number allows results to be obtained for any input A . The parameterization by Frankfurt, Guzey and Strikman, denoted FGS, combines Gribov theory with hard diffraction [21]. It is based on the CTEQ5M [22] parton densities and evolves each parton species separately to NLO for $4 < Q^2 < 10^4$ GeV. Although the x range is $10^{-5} < x < 0.95$, the sea quark and gluon ratios are unity for $x > 0.2$. The EKS98 valence quark shadowing ratios are used as input since Gribov theory does not predict valence shadowing. The parameterization is available for four different values of A : 16, 40, 110 and 206. We use the $A = 206$ parameterization for the gold nucleus.

We now turn to the spatial dependence of the shadowing. Since some qualitative spatial dependence has been observed [23] but the exact behavior is unknown, we use two different

parameterizations for inhomogeneous shadowing in d+Au collisions [11,24–26]. The first, $S_{\text{P,WS}}$, assumes that shadowing is proportional to the local density, $\rho_A(r)$,

$$S_{\text{P,WS}}^j(A, x, Q^2, \vec{s}, z) = 1 + N_{\text{WS}}[S_{\text{P}}^j(A, x, Q^2) - 1] \frac{\rho_A(r)}{\rho_A(0)}, \quad (6)$$

where $r = \sqrt{s^2 + z^2}$, $\rho_A(0)$ is the central density and N_{WS} is chosen so that $(1/A) \int d^2s dz \rho_A(\vec{s}, z) S_{\text{P,WS}}^j = S_{\text{P}}^j$. When $r \gg R_A$, the nucleons behave as free particles while, at the center of the nucleus, the modifications are larger than S_{P}^j .

If, instead, shadowing stems from multiple interactions of the incident parton [27], parton-parton interactions are spread longitudinally over the coherence length, $l_c = 1/2m_N x$, where m_N is the nucleon mass [28]. For $x < 0.016$, $l_c > R_A$ for any A and the incident parton interacts coherently with all the target partons in its path so that

$$S_{\text{P},\rho}^j(A, x, Q^2, \vec{s}, z) = 1 + N_\rho[S_{\text{P}}^j(A, x, Q^2) - 1] \frac{\int dz \rho_A(\vec{s}, z)}{\int dz \rho_A(0, z)}. \quad (7)$$

The integral over z includes the material traversed by the incident nucleon. The normalization requires $(1/A) \int d^2s dz \rho_A(\vec{s}, z) S_{\text{P},\rho}^j = S_{\text{P}}^j$ with $N_\rho > N_{\text{WS}}$. At large x , $l_c \ll R_A$ and shadowing is proportional to the local density, Eq. (6).

The fragmentation functions, $D_{h/k}(z_c, Q^2)$, are the probability for the production of hadron h from parton k with $z_c = p_h/p_k$. The produced partons are fragmented into charged pions, kaons and protons using the LO KKP fragmentation functions [29], fit to e^+e^- data. The final-state hadrons are assumed to be produced pairwise so that $\pi \equiv (\pi^+ + \pi^-)/2$, $K \equiv (K^+ + K^-)/2$, and $p \equiv (p + \bar{p})/2$. The equality of p and \bar{p} production obviously does not describe low energy hadroproduction well. At higher energies, however, the approximation that $p = \bar{p}$ may be more reasonable. The produced hadrons follow the parent parton direction. The minimum Q^2 in the KKP fragmentation functions is $Q_{\text{Fr0}}^2 = 2 \text{ GeV}^2$, similar to but somewhat lower than the minimum Q^2 of the shadowing parameterizations. Thus the minimum p_T of our calculations is $\sqrt{2} \text{ GeV}$. We assume the same scale in the parton densities and the fragmentation functions, $Q^2 = Q_{\text{Fr}}^2 = p_T^2$. A larger scale, p_T^2/z_c^2 , is sometimes used but at high p_T , where z_c is large, as is the case here, changing the scale does not significantly alter the calculated ratios.

The largest contribution to the total final-state charged particle production is from the charged pions, followed by the kaons. The proton contribution is the smallest even though, in d+Au collisions at RHIC, $(p + \bar{p})/h \approx 0.24 \pm 0.02$ where $h = h^+ + h^-$ for $2 < p_T < 3$ GeV, independent of centrality [30]. The d+Au result is similar to that from pp , 0.21 ± 0.01 [30]. The discrepancy between the RHIC d+Au and pp results and the extrapolation from e^+e^- is due to the poor knowledge of the fragmentation functions at large z_c .

We have calculated the p_T distributions for final-state charged pions, kaons and protons/antiprotons separately as well as the sum of all charged particles. For each final-state hadron, we determine the fraction of the total from produced quarks, antiquarks and gluons. In the central η bin for pion production, gluons are produced almost equally in the $gg \rightarrow gg$ and $qg \rightarrow qg$ channels. The qg channel is somewhat larger for $p_T > 5$ GeV. There is a negligible contribution from $q\bar{q} \rightarrow gg$. Pion production by quarks and antiquarks proceeds mainly through the $qg \rightarrow qg$ and $qq' \rightarrow qq'$ channels for quarks and $\bar{q}g \rightarrow \bar{q}g$, $\bar{q}q' \rightarrow \bar{q}q'$ for antiquarks. The $qq' \rightarrow qq'$ and $qg \rightarrow qg$ channels contribute nearly equally to pion production by quarks, followed by $q\bar{q} \rightarrow q\bar{q}$ and $gg \rightarrow q\bar{q}$ with a negligible contribution from $q\bar{q} \rightarrow q'\bar{q}'$. The order of importance is reversed for pion production by antiquarks. Similar results are found for kaon and proton production.

The relative contributions from the production channels changes as rapidity increases. At $\eta = 1$, the qg channel no longer dominates quark and antiquark production at $p_T > 5$ GeV. The qg , qq' and qg channels contribute almost equally to pion production by quarks while, for pions from antiquarks, the $\bar{q}g$, $\bar{q}q'$ and $q\bar{q}$ scattering channels are very similar. Here the $qg \rightarrow qg$ contribution at high p_T is larger than at midrapidity. The trend continues as η rises until, at $\eta = 3.2$, the qq' and qg scattering channels are larger than the qg for quark production while the $q\bar{q}'$ and $q\bar{q}$ scattering channels are largest for antiquark production. The qg channel dominates relative to gg for gluon production over all p_T at high η . This may seem counterintuitive since the ion x_2 value decreases as η grows, increasing the gluon density. However, the deuteron x_1 value increases more rapidly and, at large η , we are in a region where the deuteron gluon density is dropping steeply while the quark density,

particularly that of the valence quarks, is still significant. Thus the qg channel is more important than the gg channel at large η , particularly when p_T and x_1 are large.

At $|\eta| \leq 0.2$ and at $\eta = 1$, the ratios of pions, kaons and protons produced by final-state gluons, quarks and antiquarks are similar. Pion production is dominated by produced gluons up to $p_T > 10$ GeV where pions from quarks become as important. Gluons also dominate low p_T production of kaons and protons but, at $p_T \sim 3$ and 5 GeV respectively, quarks begin to dominate. Antiquark production of final-state hadrons is small. At more forward η , the situation is different. At $\eta = 2.2$, gluons dominate pion production until $p_T \sim 8$ GeV while they dominate kaon and proton production until $p_T \sim 2.5$ and 4 GeV, respectively. At high p_T , kaon and proton production by antiquarks exceeds their production from gluons at $p_T \approx 3.5$ and 6 GeV, respectively. Finally, at $\eta = 3.2$, where we reach the edge of available phase space at $p_T \approx 10$ GeV, gluons dominate pion production only until $p_T \approx 5$ GeV. Kaon and proton production is dominated by quarks at all p_T . The antiquark contribution is greater than that of gluons for protons at high η .

The p_T distributions are harder at central η values but decrease more rapidly with p_T at the largest η since at high p_T and high η we approach the edge of phase space. The low p_T contribution increases somewhat with η , in part due to the decreasing x_2 values as η increases. We have calculated the average Au ion momentum fraction, $\langle x_2 \rangle$, and the average deuteron momentum fraction, $\langle x_1 \rangle$, for $\sqrt{2} \leq p_T \leq 12$ GeV. The largest accessible p_T decreases to 10 GeV for $\eta = 3.2$ due to phase space. The results are shown in Table I. Since these are average x_2 values, the actual x_2 for each event can be smaller or larger than these averages. The minimum and maximum $\langle x_2 \rangle$ correspond to the lowest and highest p_T values respectively. Both the minimum and maximum values decrease as η increases so that the minimum $\langle x_2 \rangle$ is reached at $\eta = 3.2$. However, the maximum $\langle x_2 \rangle$ increases relative to more central η values due to the reduction of phase space at high p_T .

The total hadron yield closely follows that of the pions. There is little variation of $\langle x_2 \rangle$ between hadron species. A small difference between the partonic contributions to hadron production can be attributed to the behavior of the parton distribution functions in the

various production channels. A set of LO parton densities derived including the GLRMQ recombination terms at low x found deviations from normal DGLAP evolution at $x < 10^{-3}$ for the proton [31]. Thus one may question whether saturation effects can be at work here.

While the average Au momentum fraction is decreasing with centrality, the average deuteron momentum fraction, x_1 , is increasing. Note that the maximum $\langle x_1 \rangle$ at $\eta = 3.2$ goes to 1, indicative of the edge of phase space. The average z_c in the fragmentation functions is large and increasing with η and p_T . The fragmentation functions are best determined for smaller z_c so that the high z_c fragmentation functions are unreliable, especially for baryon production. Modeling of high p_T and high η hadron production thus contains large theoretical uncertainties due to the fragmentation functions. There is more variation in $\langle z_c \rangle$ due to parton type than in $\langle x_2 \rangle$.

We now compare the ratios, R_{dAu} , calculated for the two homogeneous shadowing parameterizations, to the BRAHMS data [8]. The EKS98 results are shown for each η interval in Fig. 1 while those employing the FGS parameterization are shown in Fig. 2. We show the results for charged pions (dashed), charged kaons (dot-dashed) and protons/antiprotons (dotted) separately. The solid curves give the total charged hadron result. At midrapidity, where $\langle x_2 \rangle$ is relatively large, the two parameterizations give rather similar results. As pointed out in Ref. [32], the difference between the kaon and proton ratios is due to isospin effects. Since the pions, which dominate the total, are predominantly produced by gluons, they are essentially independent of isospin. The ratio is greater than unity but smaller than the BRAHMS result at midrapidity. Including p_T broadening would increase the $|\eta| \leq 0.2$ ratio.

At $\eta = 1$ and low p_T , the ratio is less than unity for both parameterizations but the stronger gluon shadowing in the FGS parameterization reduces R_{dAu} to ~ 0.65 for $p_T = \sqrt{2}$ GeV relative to ~ 0.85 for EKS98. At $p_T \sim 3$ GeV, R_{dAu} rises above unity again. The trend continues to the higher rapidities until at $\eta = 3.2$, the total charged hadron ratio is less than unity for all p_T . The EKS98 parameterization tends to underestimate the data near central rapidities, Fig. 1(a) and (b). At higher η , Fig. 1(c) and (d), the calculations lie within the

uncertainties of the data, albeit above their centroids. The FGS parameterization, on the other hand, agrees rather well with the central η data, Fig. 2(a) and (b). The total charged hadron data at forward η are actually overestimated by the FGS parameterization, Fig. 2(c) and (d). Indeed, the data are in better agreement with the calculated proton/antiproton ratios than the pion-dominated total multiplicity of negatives. Thus while both shadowing parameterizations are in qualitative agreement with the data, the FGS parameterization is in somewhat better agreement than EKS98.

Figures 3 and 4 illustrate the centrality dependence of the inhomogeneous shadowing results with the FGS parameterization. We compare the central-to-peripheral ratio, R_{CP} , for the two inhomogeneous shadowing parameterizations, $S_{\text{FGS,WS}}$ in Fig. 3 and $S_{\text{FGS},\rho}$ in Fig. 4, to the BRAHMS data. The solid curves show the ratio of the central, (0 – 20)%, to peripheral, (60 – 80)%, bins for each η region while the dashed curves show the semi-central, (30 – 50)%, to peripheral ratios. Our calculations assume exact impact parameter cuts while, experimentally, impact parameter is poorly measured on an event-by-event basis.

In central collisions, with small impact parameter, inhomogeneous shadowing is stronger than the homogeneous result. The larger the homogeneous shadowing effect, the larger the difference between S_{P} and $S_{\text{P,S}}$. Thus R_{CP} is a stronger function of impact parameter for the FGS parameterization since it has larger homogeneous shadowing at small x . The ratios with $S_{\text{EKS,S}}$ underestimate the centrality dependence considerably. Note that R_{CP} approaches unity at large p_T since the difference between S_{P} and $S_{\text{P,S}}$ decreases as x increases and the shadowing effect becomes small.

The impact parameter dependence is rather weak for $S_{\text{FGS,WS}}$, shown in Fig. 3, due to the slow variation of $\rho_{\text{Au}}(r)$ with r for $r < R_{\text{Au}}$. On the other hand, $S_{\text{FGS},\rho}$ increases more smoothly with impact parameter so that the b dependence of R_{CP} is stronger. The fluctuations in R_{CP} for $S_{\text{FGS},\rho}$, especially notable at central rapidity, are due to the discrete steps of $T_{\text{Au}}(r)$ in the integration over the spatial coordinates. These fluctuations are absent for $S_{\text{FGS,WS}}$ since $\rho_{\text{Au}}(r)$ is a smooth function.

The agreement with the data is fair for $S_{\text{FGS},\rho}$ at central η , see Fig. 4(a) and (b). However,

the increase in $\langle x_2 \rangle$ with p_T results in the strong growth of R_{CP} with p_T at forward η . The resulting curvature of the calculated ratio is opposite that of the data, particularly for $\eta = 3.2$. The magnitude of R_{CP} at low p_T still agrees relatively well with the data. Since the position dependence of inhomogeneous shadowing is not well understood, the poorer agreement with the centrality-dependent data in Figs. 3 and 4 compared to the minimum bias results in Figs. 1 and 2 is not surprising. These data could be used to tune the position dependence of shadowing.

In summary, we find that the suppression factor, R_{dAu} , calculated with leading-twist shadowing, especially employing the FGS parameterization, agrees rather well with the BRAHMS data. These calculations imply that saturation effects may not play a dominant role in the forward region at RHIC, as suggested in other recent work [33]. The magnitude of the centrality dependence is reproduced at low p_T but our calculations show a stronger p_T dependence than that suggested by BRAHMS, likely due to insufficient data on the impact parameter dependence of nuclear shadowing.

We thank K.J. Eskola and V. Guzey for providing the shadowing routines and S. R. Klein and M. Murray for discussions. This work was supported in part by the Division of Nuclear Physics of the Office of High Energy and Nuclear Physics of the U. S. Department of Energy under Contract Number DE-AC03-76SF0098.

REFERENCES

- [1] K. Adcox *et al.* [PHENIX Collaboration], Phys. Lett. B **561**, 82 (2003) [arXiv:nucl-ex/0207009]; Phys. Rev. Lett. **88**, 022301 (2002) [arXiv:nucl-ex/0109003].
- [2] S. S. Adler *et al.* [PHENIX Collaboration], Phys. Rev. Lett. **91**, 072301 (2003) [arXiv:nucl-ex/0304022]; Phys. Rev. C **69**, 034910 (2004) [arXiv:nucl-ex/0308006].
- [3] C. Adler *et al.* [STAR Collaboration], Phys. Rev. Lett. **89**, 202301 (2002) [arXiv:nucl-ex/0206011].
- [4] J. Adams *et al.* [STAR Collaboration], Phys. Rev. Lett. **91**, 172302 (2003) [arXiv:nucl-ex/0305015].
- [5] I. Arsene *et al.* [BRAHMS Collaboration], Phys. Rev. Lett. **91**, 072305 (2003) [arXiv:nucl-ex/0307003].
- [6] S. S. Adler *et al.* [PHENIX Collaboration], Phys. Rev. Lett. **91**, 072303 (2003) [arXiv:nucl-ex/0306021].
- [7] J. Adams *et al.* [STAR Collaboration], Phys. Rev. Lett. **91**, 072304 (2003) [arXiv:nucl-ex/0306024].
- [8] I. Arsene *et al.* [BRAHMS Collaboration], arXiv:nucl-ex/0403005.
- [9] M. Gyulassy, P. Lévai and I. Vitev, Phys. Lett. B **538**, 282 (2002) [arXiv:nucl-th/0112071].
- [10] I. Vitev, M. Gyulassy and P. Lévai, Acta Phys. Hung. New Ser. Heavy Ion Phys. **17**, 237 (2003) [arXiv:nucl-th/0204019].
- [11] V. Emel'yanov, A. Khodinov, S. R. Klein and R. Vogt, Phys. Rev. C **61**, 044904 (2000) [arXiv:hep-ph/9909427].
- [12] R. D. Field, *Applications Of Perturbative QCD* (Addison-Wesley, Redwood City, CA, 1989).

- [13] J. F. Owens, Rev. Mod. Phys. **59**, 465 (1987).
- [14] S. R. Klein and R. Vogt, Phys. Rev. Lett. **91**, 142301 (2003) [arXiv:nucl-th/0305046].
- [15] C. W. De Jager, H. De Vries and C. De Vries, Atom. Data Nucl. Data Tabl. **14** (1974) 479.
- [16] D. Kharzeev, E.M. Levin and M. Nardi, Nucl. Phys. A **730**, 448 (2004) [arXiv:hep-ph/0212316]; L. Hulthen and M. Sagawara, in *Handbuch der Physik*, **39** (1957).
- [17] A. D. Martin, R. G. Roberts, W. J. Stirling and R. S. Thorne, Phys. Lett. B **443**, 301 (1998) [arXiv:hep-ph/9808371].
- [18] M. Gluck, E. Reya and A. Vogt, Z. Phys. C **53**, 127 (1992).
- [19] K. J. Eskola, V. J. Kolhinen and P. V. Ruuskanen, Nucl. Phys. B **535**, 351 (1998) [arXiv:hep-ph/9802350].
- [20] K. J. Eskola, V. J. Kolhinen and C. A. Salgado, Eur. Phys. J. C **9**, 61 (1999) [arXiv:hep-ph/9807297].
- [21] L. Frankfurt, V. Guzey and M. Strikman, arXiv:hep-ph/0303022.
- [22] H. L. Lai *et al.* [CTEQ Collaboration], Eur. Phys. J. C **12**, 375 (2000) [arXiv:hep-ph/9903282].
- [23] T. Kitagaki *et al.*, Phys. Lett. B **214**, 281 (1988).
- [24] V. Emel'yanov, A. Khodinov, S. R. Klein and R. Vogt, Phys. Rev. C **56**, 2726 (1997) [arXiv:nucl-th/9706085].
- [25] V. Emel'yanov, A. Khodinov, S. R. Klein and R. Vogt, Phys. Rev. Lett. **81**, 1801 (1998) [arXiv:nucl-th/9805027].
- [26] V. Emel'yanov, A. Khodinov, S. R. Klein and R. Vogt, Phys. Rev. C **59**, R1860 (1999) [arXiv:hep-ph/9809222].

- [27] A. L. Ayala, M. B. Gay Ducati and E. M. Levin, Nucl. Phys. B **493**, 305 (1997) [arXiv:hep-ph/9604383].
- [28] Z. Huang, H. Jung Lu and I. Sarcevic, Nucl. Phys. A **637**, 79 (1998) [arXiv:hep-ph/9705250].
- [29] B. A. Kniehl, G. Kramer and B. Pötter, Nucl. Phys. B **582**, 514 (2000) [arXiv:hep-ph/0010289].
- [30] J. Adams *et al.* [STAR Collaboration], arXiv:nucl-ex/0309012.
- [31] K. J. Eskola, H. Honkanen, V. J. Kolhinen, J. w. Qiu and C. A. Salgado, Nucl. Phys. B **660**, 211 (2003) [arXiv:hep-ph/0211239].
- [32] S. R. Klein and R. Vogt, Phys. Rev. C **67**, 047901 (2003) [arXiv:nucl-th/0211066].
- [33] J. Jalilian-Marian, arXiv:hep-ph/0402080.

TABLES

η	$\langle x_2 \rangle$		$\langle x_1 \rangle$		$\langle z_c \rangle$	
	min	max	min	max	min	max
≈ 0	0.1	0.3	0.1	0.3	0.3	0.5
1	0.02	0.15	0.3	0.45	0.3	0.6
2.2	0.01	0.1	0.35	0.7	0.35	0.8
3.2	0.005	0.2	0.5	1.0	0.55	1.0

TABLE I. The average values of the Au and d momentum fractions, $\langle x_2 \rangle$ and $\langle x_1 \rangle$ respectively, as well as the average fraction of the final-state parton momentum transferred to the hadron, $\langle z_c \rangle$, in the four BRAHMS pseudorapidity intervals. The minimum values correspond to $p_T \approx \sqrt{2}$ GeV while the maximum corresponds to $p_T = 12$ GeV for the first three η bins and 10 GeV for the most forward η bin.

FIGURES

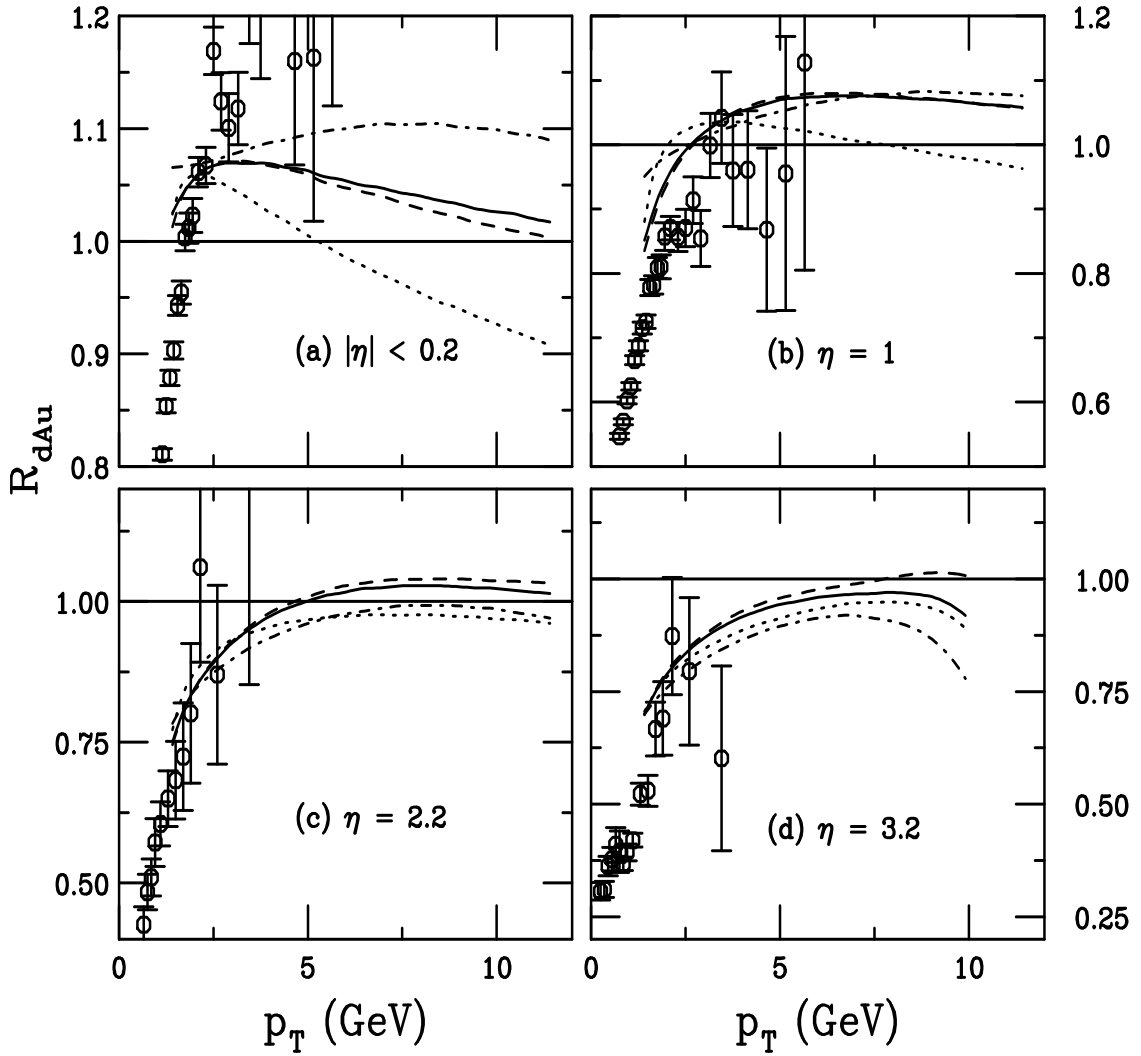


FIG. 1. R_{dAu} for charged pions (dashed) and kaons (dot-dashed) as well as protons and antiprotons (dotted) and the sum over all charged hadrons (solid) for deuteron-gold collisions at $\sqrt{S_{NN}} = 200$ GeV as a function of p_T . The results for homogeneous shadowing with the EKS98 parameterization are compared to the BRAHMS data [8] in the following η bins: (a) $|\eta| \leq 0.2$; (b) $\eta = 1$; (c) $\eta = 2.2$ and (d) $\eta = 3.2$.

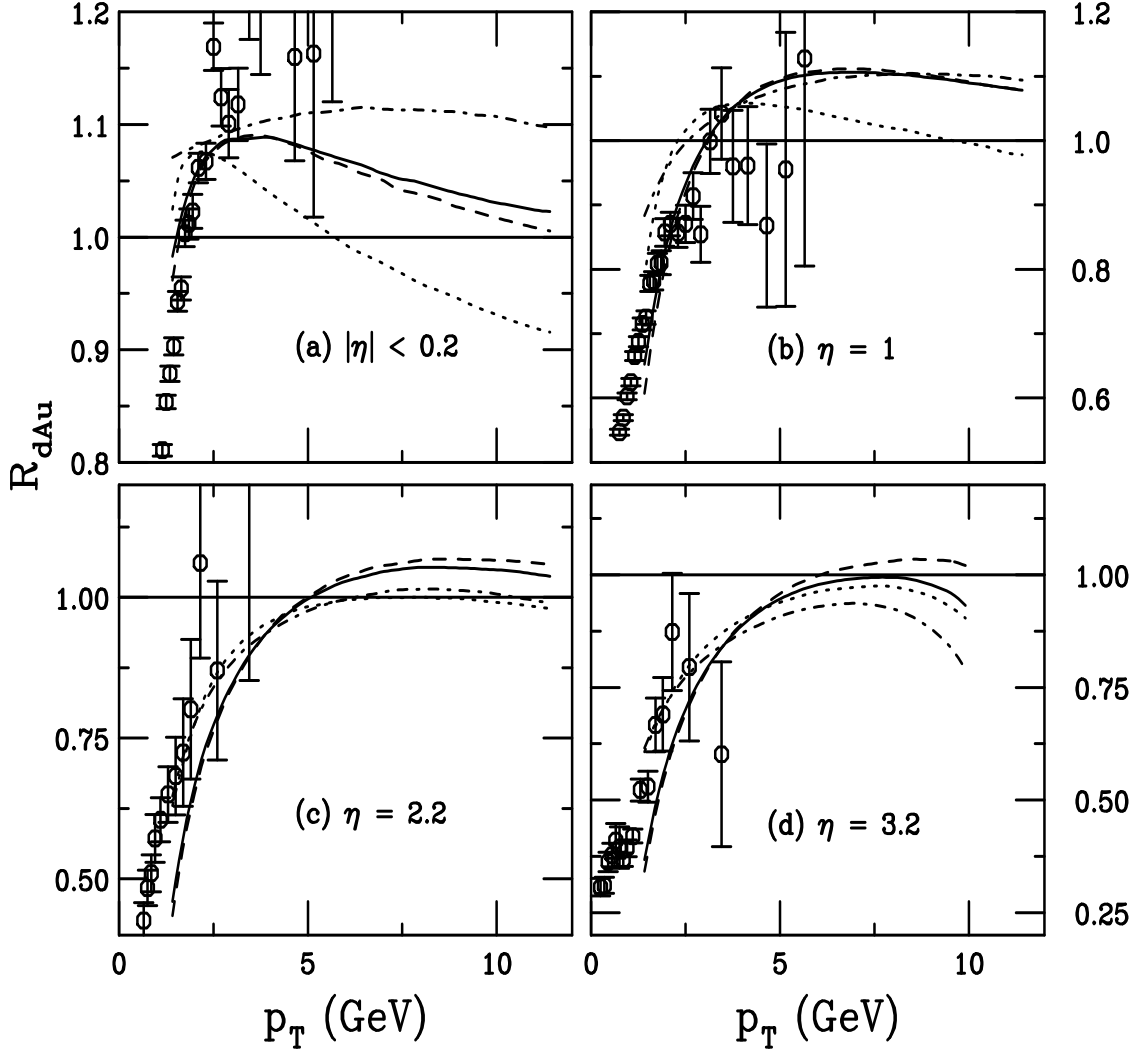


FIG. 2. R_{dAu} for charged pions (dashed) and kaons (dot-dashed) as well as protons and antiprotons (dotted) and the sum over all charged hadrons (solid) for deuteron-gold collisions at $\sqrt{S_{NN}} = 200$ GeV as a function of p_T . The results for homogeneous shadowing with the FGS parameterization are compared to the BRAHMS data [8] in the following η bins: (a) $|\eta| \leq 0.2$; (b) $\eta = 1$; (c) $\eta = 2.2$ and (d) $\eta = 3.2$.

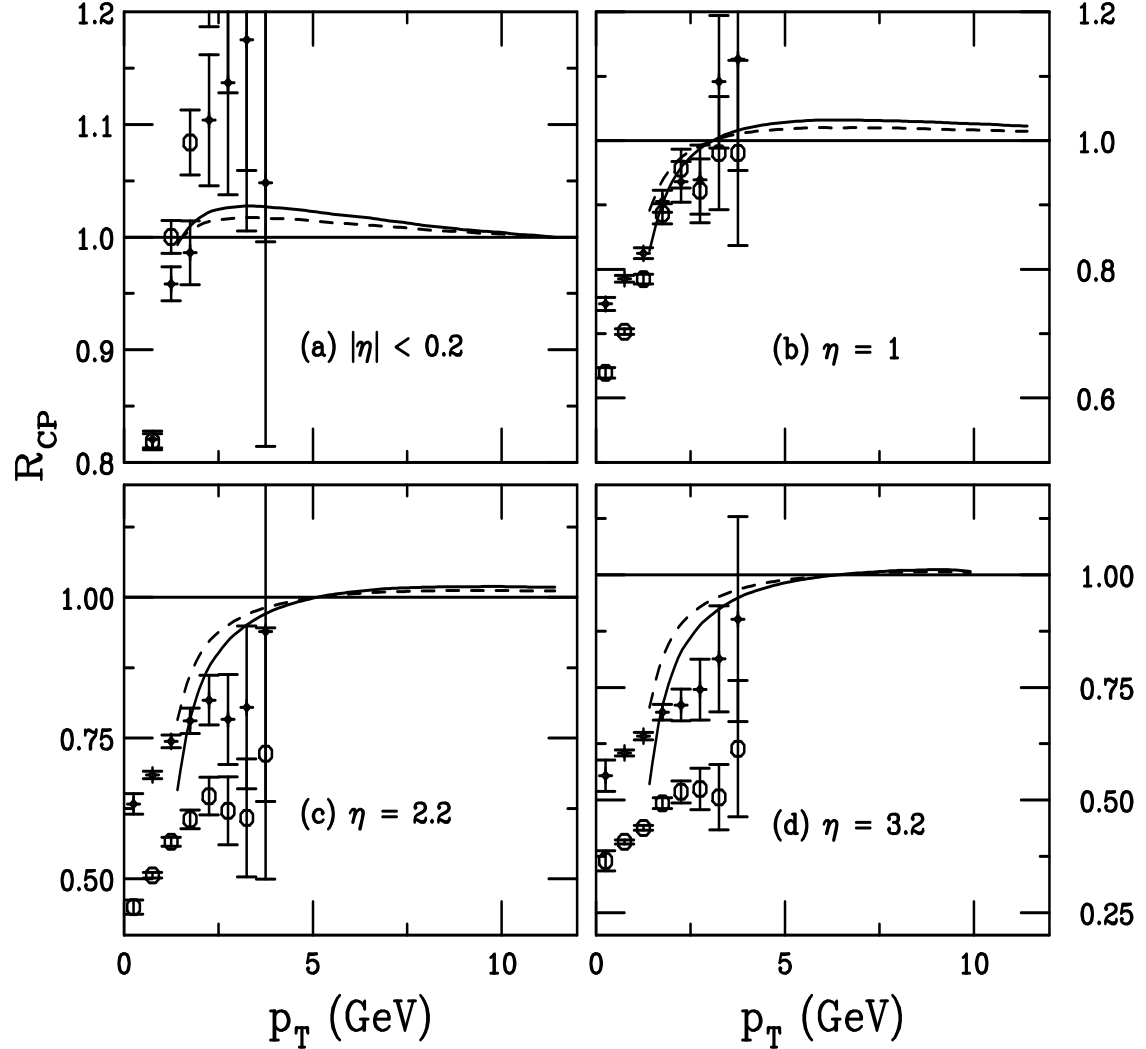


FIG. 3. R_{CP} for charged hadrons in deuteron-gold collisions at $\sqrt{S_{NN}} = 200$ GeV as a function of p_T . The results for $S_{FGS,WS}$ are compared to the BRAHMS data [8] in the following η bins: (a) $|\eta| \leq 0.2$; (b) $\eta = 1$; (c) $\eta = 2.2$ and (d) $\eta = 3.2$. The calculated ratios of the most central and semi-central to peripheral collisions are shown in the solid and dashed curves, respectively. The BRAHMS data are given by the open circles (most central) and diamonds (semi-central).

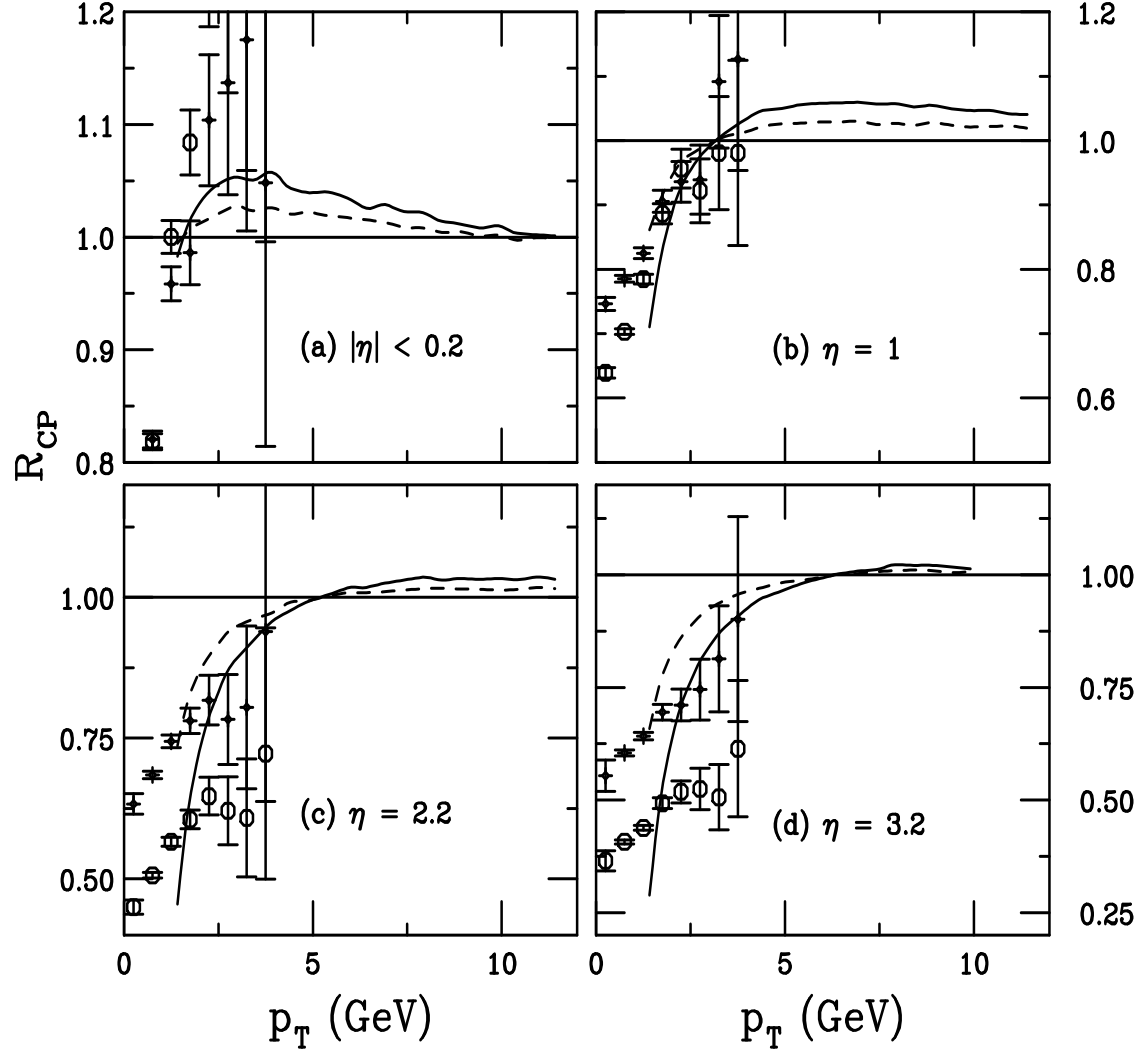


FIG. 4. R_{CP} for charged hadrons in deuteron-gold collisions at $\sqrt{S_{NN}} = 200$ GeV as a function of p_T . The results for $S_{FGS,\rho}$ are compared to the BRAHMS data [8] in the following η bins: (a) $|\eta| \leq 0.2$; (b) $\eta = 1$; (c) $\eta = 2.2$ and (d) $\eta = 3.2$. The calculated ratios of the most central and semi-central to peripheral collisions are shown in the solid and dashed curves, respectively. The BRAHMS data are given by the open circles (most central) and diamonds (semi-central).